**JOURNAL OF FUEL CHEMISTRY AND TECHNOLOGY**
Volume 46, Issue 11, November 2018
Online English edition of the Chinese language journal

Available online at www.sciencedirect.com
ScienceDirect

**Cite this article as:** J Fuel Chem Technol, 2018, 46(11), 1332−1341

RESEARCH PAPER

# Ni-based catalysts obtained from perovskites oxides for ethanol steam reforming

**Fabiola Nerina Agüero[1], Jose Antonio Alonso[2], Maria Teresa Fernández-Díaz[3], Luis Eduardo Cadus[1,*]**

[1]Instituto de Investigaciones en Tecnología Química (INTEQUI), UNSL-CONICET, Almirante Brown 1455, 5700 San Luis, Argentina;
[2]Instituto de Ciencia de Materiales de Madrid, Consejo Superior de Investigaciones Científicas, Cantoblanco, 28049 Madrid, Spain;
[3]Institut Laue-Langevin, B.P. 156, F-38042 Grenoble Cedex 9, France

**Abstract:** Perovskites as host structures of cations were used in order to generate in situ active and stable catalysts for ethanol steam reforming. For this purpose, $La_{1-x}Mg_xAl_{1-y}Ni_yO_3$ ($x$ = 0.1; $y$= 0, 0.1, 0.2, 0.3) perovskites were synthetized by the citrate method. Ni segregation is evident for a substitution level higher than 0.2. The segregation of Ni as NiO generated species interacts with different metal-support after the reduction step. The $y$= 0.1 catalyst presents the highest $H_2$ yield value about 85% during reaction time, with low mean values of $CH_4$ and CO selectivities of 3.4% and 11%, respectively and a low carbon formation. The better performance of $y$= 0.1 catalyst could be attributed to the minor proportion of segregated phases, thus a controlled expulsion of Ni is successfully reached.

**Key words:** perovskites; catalyst design; ethanol; steam reforming

It is known that catalysts provide low-energy pathways for converting chemical species and have been extensible used for the production of chemicals at industrial level[1]. There are several benefits in using catalytic processes, however, obtaining an efficient catalyst for a specific process is still a challenge. The need to obtain an economically viable catalyst with high catalytic activity and stability makes imperative the use of design criteria. A catalyst design not only must consider the separate effects of the active sites and support, but also should include the interaction between them[2]. In this sense the study of perovskite type solids as precursors of metal catalysts becomes interesting. Perovskite is a well-defined mixed oxide solid with general chemical formula of $ABO_3$, whereby $A$ site is lanthanide metal and $B$-site is a transitional metal. This structure admits the inclusion by substitution of other elements $A'$ or $B'$ which results interesting in order to find the desired physico-chemical features with high thermal stability and catalytic activity[3,4]. The exosolution of $B$' is favoured in comparison of $B$ on the basis of their metallic character. In fact, when this structure is submitted to a high temperature reducing atmosphere a catalyst with large amounts of nano-size metal particles homogeneously dispersed in an inorganic matrix is obtained.

These advantages make this structure suitable to be used as precursor of catalysts used in structure sensitive reactions. A possible application of these solids is the steam reforming reaction. In recent years, ethanol steam reforming has become one of major processes for hydrogen production. Thermodynamic and reaction mechanisms of ethanol steam reforming reaction have been widely studied. There is vast information about this reaction and characterization of the catalytic centres. Therefore, it is possible to take this information to select $A'$ and $B'$ cations in order to try to design a catalyst. Hydrogen production depends on the different reaction pathways. Several undesired by-products as CO, $CH_4$, $C_2H_4$, $CH_3CHO$, and coke, could be obtained depending on the reaction involved[5]. Therefore, it is important to ensure sufficient amount of water steam and minimize the dehydration and decomposition of ethanol to maximize the production of hydrogen. Catalysts play a critical role in order to obtain total ethanol conversion and high hydrogen yield. Noble metals such as Rh, Ru, Pt, Pd and Ir have been widely investigated considering that all these metals present high C–C bond cleavage capacity[6–12]. The search for alternative catalysts is also driven by the high cost of noble metals. Thus, Ni has been proposed as an alternative catalyst after noble metals in reforming reactions due to its ability to promote the breaking of this bond[13,14].

Received: 29-Jun-2018; Revised: 19-Sep-2018.
Corresponding author. E-mail: lcadus@unsl.edu.ar.

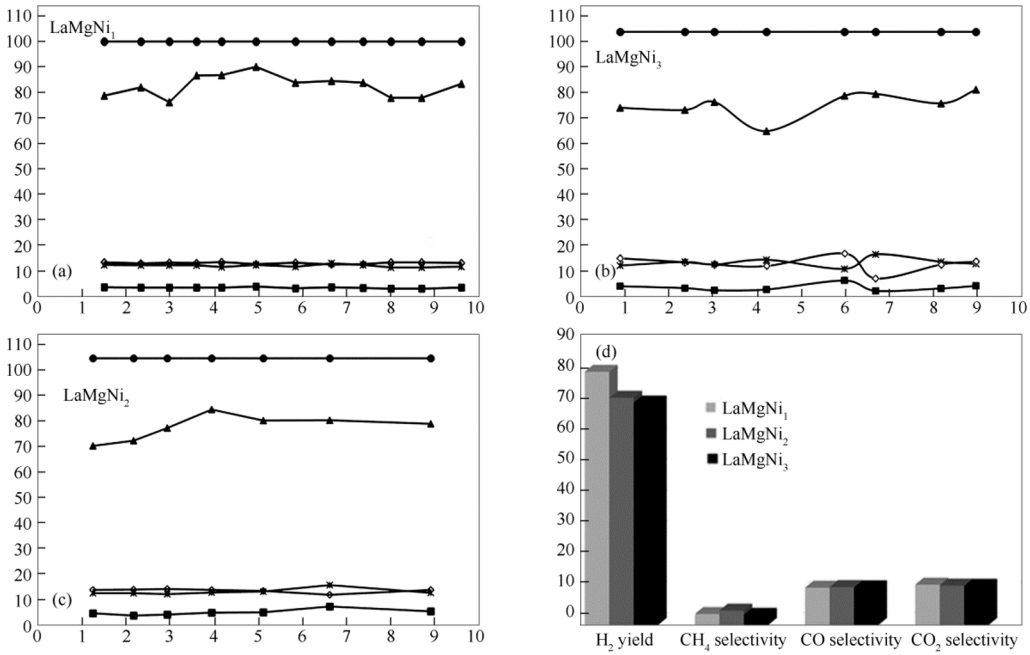


Fig. 1 Catalytic performance of perovskite catalysts during 9 h on stream

●: ethanol conversion; ▲: $H_2$; ✳: CO selectivity; ◇: $CO_2$ selectivity; ■: $CH_4$ selectivity

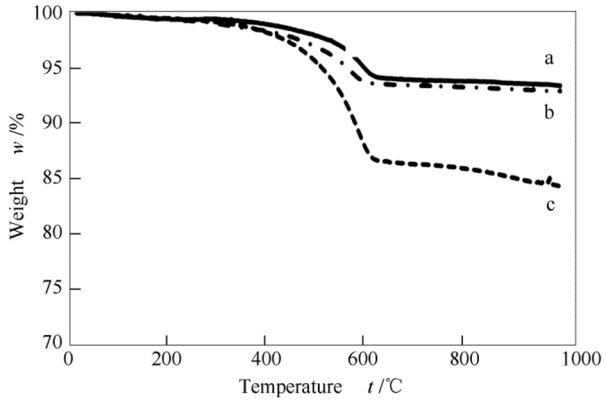


Fig. 2 TG results of catalysts used in ethanol steam reforming reaction

a: $LaMgNi_1$; b: $LaMgNi_2$; c: $LaMgNi_3$

Besides the active phase, the support can interact with ethanol modifying the catalyst activity. By partially substituting the *A*-site with alkaline earth metal oxide, the perovskite catalyst can have more basic sites. It is known that acid sites favour the reaction of ethanol dehydration, which can lead to a progressive deactivation of the catalyst by carbon formation[15]. An essential requirement for these studies is to use synthesis methods to ensure a defined structure and high purity. The high purity of these materials is essential to discriminate the origin of cations expulsed to the surface. In addition, the selected synthesis method should allow controlling the particle size in nanometric scale. Since large particles facilitate the formation of carbon leading to the deactivation of catalyst[13]. The formation of carbonaceous deposits is a structure sensitive reaction, and thus controllable with the domain size of Ni centres. Bengaard et al[16] have reported a critical size below which the formation of coke can be prevented and additives such as K, S and Au catalyst can give more tolerance to carbon formation. According to a model proposed by Borowecki[17] there is a relationship between the domain size of the Ni catalytic centre and the rate of formation of coke. Thus, it is essential to use design criteria during the synthesis of catalysts, since the activity, selectivity and stability are affected by the nature of the metal particle, the support and the interaction between them.

In a previous paper[18], $La_{1-x}Ca_xAl_{1-y}Ni_yO_3$ ($x$ = 0, 0.1; $y$=0, 0.1, 0.2, 0.3) perovskite type oxides were studied. These catalysts presented an excellent catalytic activity in ethanol steam reforming reaction. The effect of the addition of an alkaline metal in the *A* site of perovskites with the aim to avoid the ethanol dehydrogenation reaction and thus carbon formation was investigated. However, no significant differences in products selectivities were observed, which could indicate that Ca did not induce changes in reaction mechanism. Moreover, it could be demonstrated that the presence of Ca in the perovskite avoided total inclusion of Ni in the structure. For this reason, in this work it was decided to study the effect of the addition of Mg, another alkaline metal with a smaller radius, which could give the suitable basic character and it could probably allow a complete insertion of Ni in the structure. The purity of the prepared catalysts is necessary in order to control the expulsion of cations after the reduction process.

Table 1 BET specific surface area, $H_2$ consumption from TPR, Ni content from ICP-OES and weight loss from TG

| Catalyst | $A_{BET}$/($m^2 \cdot g^{-1}$) | $H_2$ consumption/(μmol·$mg^{-1}$(Ni)) | Ni content *w*/% | Weight loss *w*/% |
|---|---|---|---|---|
| $LaAlO_3$ | 14 | – | – | |
| $La_{0.9}Mg_{0.1}AlO_3$ | 15 | – | – | |
| $NiO/LaAlO_3$ | 17 | 0.63 | 3.3 (2.8)* | |
| $LaMgNi_1$ | 13 | 2.16 | 2.2 (2.8) | 6 |
| $LaMgNi_2$ | 10 | 2.04 | 3.4 (5.6) | 7 |
| $LaMgNi_3$ | 8 | 1.39 | 5.2 (8.3) | 15 |

*: values between brackets correspond to nominal ones

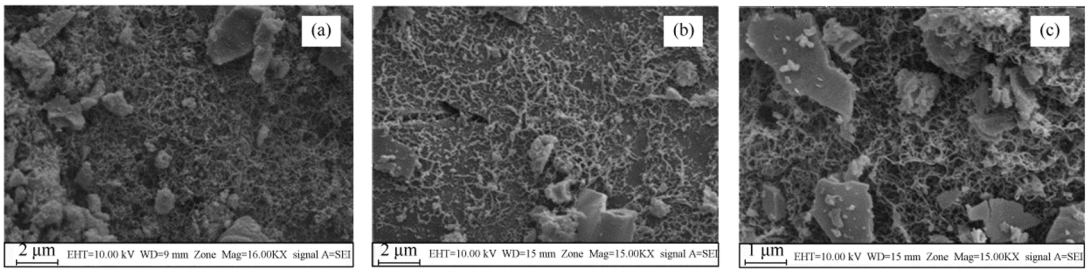


Fig. 3 SEM images of used catalysts
(a): $LaMgNi_1$; (b): $LaMgNi_2$; (c): $LaMgNi_3$

Therefore, this work is based in the use of $AA'BB'O_3$ perovskites as precursors of catalysts with a proper selection of cations with the aim to generate in situ the active phase and the support with the desired characteristics, with *A*=La, Mg and *B*=Al, Ni. The samples will be evaluated in ethanol steam reforming reaction as a validation of the theory.

## 1 Experimental

$La_{1-x}Mg_xAl_{1-y}Ni_yO_3$ ($x$ = 0.1; $y$=0, 0.1, 0.2, 0.3) perovskites were synthetized by the citrate method[19]. Metal nitrates were dissolved in a lowest water quantity separately. In a round-bottom flak of plane base nitrates solutions were added by one to a citric acid solution (10% in excess) and agitated during 15 min. The resulting solution was concentrated with a slowly evaporation in a rotavapor at 75°C under vacuum until a gel was obtained. This gel was dried at 200°C overnight in a vacuum stove, producing a solid amorphous precursor. The resulting precursor was milled and calcined in air at 800°C for 2 h. The samples were named $LaMgNi_y$ with $y$=1, 2, 3. Additionally, a reference catalyst $NiO/LaAlO_3$ was prepared by impregnation incipient wetness with $Ni(NO_3)_2$ aqueous solution. The amount of $Ni(NO_3)_2$ was the necessary to obtain a nickel loading equivalent to $LaMgNi_1$ catalyst.

### 1.1 Catalysts characterization

BET specific surface areas ($A_{BET}$) of samples were calculated by the BET method. A Gemini V from Micromeritics apparatus was used. Samples were degassed overnight at 350°C. X-ray diffraction (XRD) patterns were obtained with a Rigaku diffractometer operated at 30 kV and 25 mA using Cu $K\alpha$ radiation with Nickel filter ($\lambda$ = 0.15418 nm). Inductively coupled plasma (ICP) was used to determinate the elemental composition of catalysts. An ELAN DRC-e ICP-MS apparatus was used. Samples were previously dissolved using a START D microwave digestion system. X-ray photoelectron spectroscopy (XPS) was recorded with A Multitecnic UniSpecs equipment with a dual X ray source of Mg/Al and a hemispheric analyzer PHOIBOS 150 was used to obtained XPS data. The pressure was kept under $2.9\times10^{-8}$ kPa. The samples were previously reduced at 600°C in 50 mL/min 5% of $H_2/N_2$ stream. Temperature programmed reduction (TPR) was performed in a quartz tubular reactor using a TCD detector. Samples of 100 mg were reduced with a mixture of 5% $H_2/N_2$, at a total flow rate of 30 mL/min. The temperature was increased at a rate of 10°C/min from room temperature to 700°C. Neutron power diffraction (NPD) was recorded in the D2B diffractometer at the Institute Laue Langevin (ILL)-Grenoble at room temperature (RT). The high-intensity mode ($\Delta d/d \geq 2\times10^{-3}$) was selected with a neutron wavelength $\lambda$ = 0.1594 nm over the angular range $0.1° < 2\theta < 160°$ with a 0.05° step. Approximately 2 g of each sample were contained in a vanadium sample holder. The NPD patterns were analyzed by the Rietveld method[20] with the Fullprof program[21]. A pseudo-Voigt function was considered to generate the profile shape. The background was fit to a 5th-degree polynomial.

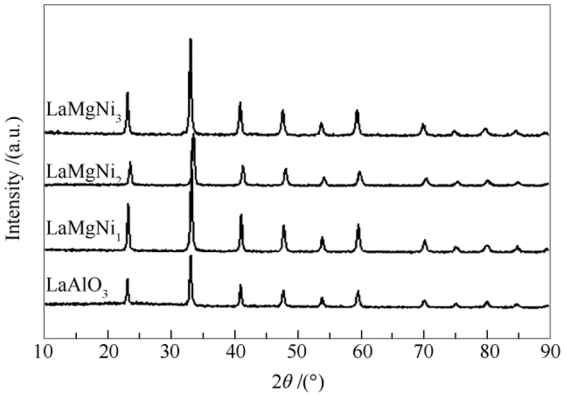


Fig. 4 X-ray diffraction patterns of samples calcined at 800°C

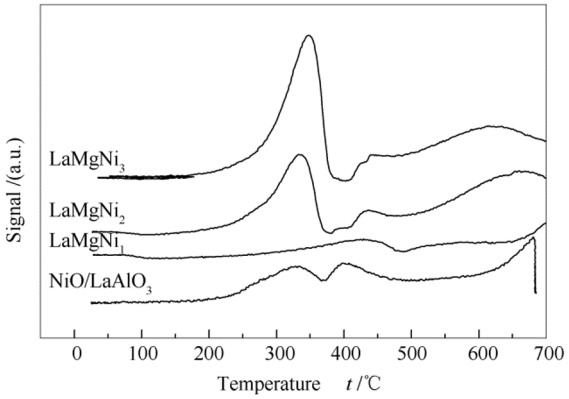


Fig. 5 $H_2$-TPR profiles of $LaMgNi_1$, $LaMgNi_2$, $LaMgNi_3$ and $NiO/LaAlO_3$

The coherent scattering lengths used for La, Mg, Al, Ni, and O were: 8.24, 5.375, 3.44, 10.300, and 5.803 fm, respectively. Scanning electron microscopy (SEM) images were obtained with a LEO 1450 VP scanning electron microscope provided with energy dispersive X-ray analysis (EDAX) equipment for the quantitative analysis. Thermogravimetric analysis was carried out in a Shimadzu, DTG-60 model thermobalance. 10 mg samples were heated from ambient temperature up to 1000°C at a heating rate of 10°C/min under 50 mL/min of synthetic air.

### 1.2 Catalytic tests

The ethanol steam reforming reaction was carried out in a quartz fixed-bed reactor loaded with 150 mg catalyst (35–50 mesh) mixed with 1000 mg quartz particles. The samples were previously reduced at 600°C *in situ* with 50 mL/min of 5% $H_2/N_2$ for 1 h, followed by purging at the same temperature with 50 mL/min of He during 30 min. The liquid solution was fed with a pump (Eldex) into a heated chamber (150°C) to completely evaporate the solution in the stream of He before reaction. A WHSV $3.3\times10^{-4}$ $mL_{liq}/(mg_{cat}\times min)$ was used with 50 mL/min of helium as carrier. The reaction temperature was 600°C under atmospheric pressure. The composition of the non condensable fraction of the stream was quantified by a GC (Shimadzu) equipped with a Carbosphere column, whereas condensable materials were quantified by GC (Buck Scientific) with a Porapak Q column, both provided with a thermal conductivity detector (TCD).

Ethanol conversion ($x_{EtOH}$), selectivity to carbon products ($s_j$); and hydrogen yield $\eta_{H_2}$ were calculated as follows:

$$x_{EtOH}\ (\%) = 100\times(F_{EtOH,in} - F_{EtOH,out}) / (F_{EtOH,in}) \quad (1)$$

$$\eta_{H_2}\ (\%) = 100\times F_{H_2,out} / (6\times F_{EtOH,in}) \quad (2)$$

$$s_j\ (\%) = 100\times F_{j,out} / (\Sigma F_{j,out}),\ \text{with } j = CH_4, CO \text{ and } CO_2 \quad (3)$$

## 2 Results and discussion

As it is mentioned in the introduction section the objective of catalyst design is to obtain active and stable catalysts in the studied reaction. In this case the ethanol steam reforming reaction is considered as case study. Figure 1 presents the performance parameters, ethanol conversion rate, hydrogen yield and $CH_4$, CO, and $CO_2$ selectivities as a function of time. The three samples present high activity during 9 h on stream. The total conversion of ethanol for all samples is observed with high $H_2$ yields, between 70% and 80%. Acetaldehyde, ethylene and ethane are not detected in any case. This is expected since a high reaction temperature (600°C) used. It is known that ethanol steam reforming is a sequential reaction[22,23]. Dehydrogenation of ethanol generates acetaldehyde and hydrogen, acetaldehyde can further react to produce acetone and hydrogen, and acetone can be further polymerized to form coke. In another way, acetaldehyde, acetone and the coke deposited can react with water to produce methane, carbon monoxide and hydrogen. Other two main reactions are the steam reforming of methane and the water gas shift reaction, both of which produce hydrogen. Steam reforming of methane generally takes place at higher temperature, mainly above 500°C. At lower reaction temperatures, some intermediate compounds, such as acetaldehyde and acetone, could remain and thus they could be detected in the reaction products. The low $CH_4$ and CO selectivities and high $H_2$ yield that these samples present would indicate the contribution of both, methane reforming and water gas shift reactions. $LaMgNi_1$ catalyst presents the highest $H_2$ yield value, about 85%, during the reaction time, while low values of $CH_4$ and CO selectivities of 3.4% and 11%, respectively, are measured. The effect of Mg addition can be observed comparing one of these catalysts, $LaMgNi_1$ with a catalysts synthetized and presented in a previous paper[18], with an equivalent composition of Ni. This catalyst is called $LaAlNi_1$ and presents the following values as a result of the ethanol steam reforming reactions: 71% $H_2$ yield, $CH_4$, CO and $CO_2$ selectivities of 4%, 10% and 18%, respectively.

Table 2 Structural parameters for the perovskites with nominal composition $La_{0.9}Mg_{0.1}Al_{1-y}Ni_yO_3$, refined in the rhombohedral $R\bar{3}c$ (no. 167) space group at 25°C from NPD data

| Ni contents | $y$= 0.1 | $y$= 0.2 | $y$= 0.3 |
|---|---|---|---|
| $a$/Å | 5.3670(6) | 5.3735(5) | 5.3821(5) |
| $c$/Å | 13.139(2) | 13.149(2) | 13.149(2) |
| $v$/Å$^3$ | 327.75(8) | 328.79(7) | 329.86(6) |
| La/Mg | *6a* (0 0 1/4) | | |
| $f_{occ}$ La/Mg | 0.99(2)/0.01(2) | 1.00(2)/0.00(2) | 0.99(2)/0.01(2) |
| $B$/Å$^2$ | 0.36(4) | 0.36(3) | 0.31(3) |
| (Al,Ni) | *6b* (0 0 0) | | |
| $f_{occ}$ Al/Ni | 0.95(1)/0.05(1) | 0.936(4)/0.064(1) | 0.810(2)/0.190(2) |
| $B$/Å$^2$ | 0.49(6) | 0.47(5) | 0.88(3) |
| O | *18e* ($x$ 0 1/4) | | |
| $x$ | 0.4751(2) | 0.4737(2) | 0.4717(2) |
| $f_{occ}$ | 1.0 | 1.0 | 1.0 |
| $B$/Å$^2$ | 0.69(3) | 0.77(2) | 0.88(3) |
| Fraction main phase | 96.6(1) | 93.8(1) | 93.1(1) |
| Fraction MgO | 1.2(1) | 0.6(1) | 2.7(1) |
| Fraction NiO | 2.2(1) | 5.6(1) | 4.2(1) |
| Reliability factors | | | |
| $\chi^2$ | 2.20 | 5.22 | 2.22 |
| $R_p$/% | 2.82 | 2.60 | 2.82 |
| $R_{wp}$/% | 2.27 | 3.61 | 2.12 |
| $R_I$/% | 2.48 | 1.58 | 1.77 |

The presence of Mg favours the higher production of $H_2$ and $CO_2$, namely, it favours the ethanol steam reforming reaction, with a lower production of $CH_4$ and CO undesired products. Spent catalysts were characterized by TG and SEM analyses in order to study the presence or not of carbon, one of the most common undesired reaction products. The weight loss can be seen in Figure 2 and the data are listed in Table 1. The weight loss is attributed to the combustion of carbon deposition. The amount of carbon deposited increases with the increase in Ni substitution level. Indeed, $LaMgNi_3$ catalyst presents the highest weight loss (15%). It is known that different types of carbon can be found on the surface of spent catalysts, such as amorphous carbon, filamentous carbon, graphitic carbon, polymeric carbon stemming from ethylene polymerization and $CH_x$ species[24–27].

In order to characterize the nature of the carbonaceous species formed over the catalysts, the SEM analysis was carried out and the micrographs are shown in Figure 3. The images show the presence of carbon filaments over the three catalysts. It has been published that Ni particles are located at the ends of carbon filaments. Therefore, the metal remains active during ethanol steam reforming because the surface remains exposed to the reactants and therefore, the carbon formed does not result in significant catalyst deactivation. Even if differences in catalytic activity with the other catalysts are small, the better performance of $LaMgNi_1$ catalyst and the lower carbon formation are significant. Thus an exhaustive characterization of solids would be necessary in order to explain the excellent catalytic performance. The possibility that perovskite structures present to incorporate different cations at *A* and *B* sites makes them suitable to be used as precursor catalysts in steam reforming reactions. A good dispersion of the active phase could be reached by the migration of more reducible cations, in this case Ni, from the host perovskite structure to the surface, after a reduction procedure. However, a high purity of the synthetized samples is essential to corroborate the inclusion of nickel into the structure and to control its expulsion after the reduction step. The synthesis method used in this work is the citrate method, which is known to yield solids with high purity since the precursor gel is highly homogeneous. Moreover, solids prepared by this method have higher surface areas than those one obtained from other preparation methods for the same compositions. Table 1 shows the $A_{BET}$ results. The specific surface areas of samples decrease with Ni substitution level, from 13 to 8 m$^2$/g approximately. The partial substitution of sites with Mg leads to an increase of the $A_{BET}$ in comparison to the unsubstituted $LaAlO_3$ perovskite. The purity of the samples can also be analysed from XRD results. Diffractograms of calcined catalysts are shown in Figure 4.

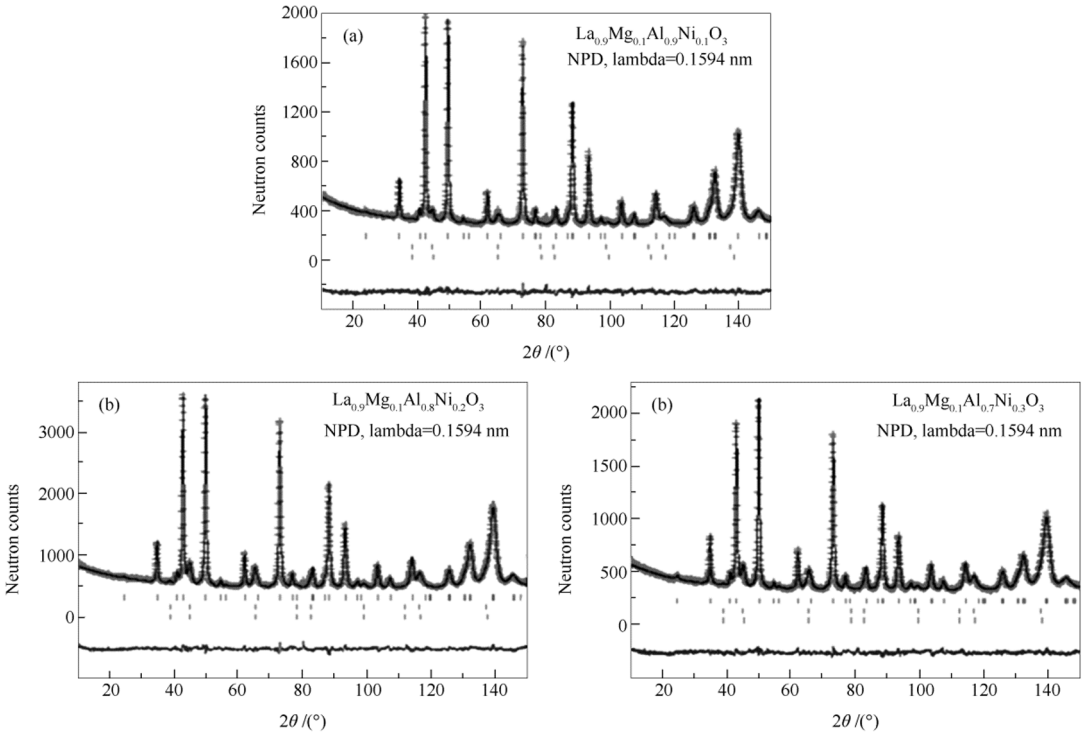


Fig. 6 Neutron powder diffraction Rietveld profiles of $LaMgNi_y$ for (a) $y$= 0.1, (b) $y$= 0.2 and (c) $y$= 0.3

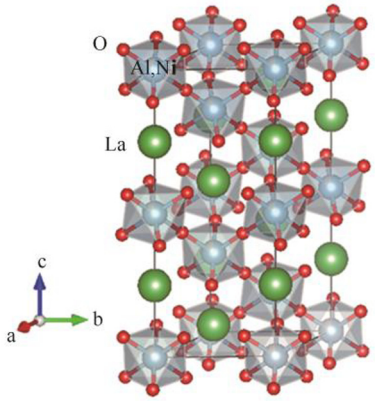


Fig. 7 A view of the crystal structure of $LaMgNi_2$ at RT, defined as a superstructure of perovskite consisting of a framework of slightly tilted (Al, Ni)O6 octahedra with La atoms in the voids

All samples show a good crystallinity and exhibit diffraction peaks corresponding to those reported for the pure $LaAlO_3$ perovskite phase (JCP.DS file 96-900-7996). The crystallinity is not modified with the substitution of Mg, nor by the higher Ni content in the B position. Diffraction peaks corresponding to $La_2O_3$, MgO, NiO, $Al_2O_3$, or other segregated phases are not observed. However, due to the limitations of this technique, it is possible to have the presence of these phases in low concentrations or in amorphous arrangements. Table 1 shows the Ni content of samples. The values are lower than the nominal ones in all cases. Ni contents increase from approximately 2% to 5% with Ni substitution level. Considering the Ni low concentration and the high crystallinity of samples, it could be deduced that the absence of diffraction lines corresponding to NiO phases could be related either to the presence of small crystallites of NiO or to the insertion of Ni into the perovskite structure. The analysis of catalysts reducibility could give more information about Ni species in the perovskite. $H_2$-TPR profiles of catalysts and a reference of $NiO/LaAlO_3$ are shown in Figure 5. This reference sample presents two reduction signals at 330 and 400°C, and another one at higher temperature that is not completely resolved due to the limitations of the equipment. The first two signals would correspond to the reduction of Ni species, which are in different levels of interaction with the support[28]. The signal at higher temperature could be attributed to the presence of oxygen vacancies in the $LaAlO_3$ perovskite[24] or to the presence of a spinel phase. It has been reported that $NiAl_2O_4$ phase presents a reduction signal above 700°C[25]. XRD data give no evidence of the presence of the spinel phase, but, as it is mentioned above, the presence of this phase cannot be discarded. $LaMgNi_1$ perovskite presents a broad reduction signal between 300 and 500°C, with a maximum at 420°C, and another signal at a temperature above 700°C. The reduction profiles of $LaMgNi_2$ and $LaMgNi_3$ perovskites present a main reduction signal at 350°C, which intensity increases with Ni content, two signals of low intensity between 400 and 450°C and also the signal above 700°C.

Table 3 Main interatomic distances (Å) and selected angles (°) for the perovskites with nominal composition $La_{0.9}Mg_{0.1}Al_{1-y}Ni_yO_3$

| Ni content | $y$=0.1 | $y$= 0.2 | $y$= 0.3 |
|---|---|---|---|
| Al,Ni)–O ×6 | 1.9018(7) | 1.9044(7) | 1.9073(8) |
| O–(Ni,Mo)–O | 90.16(4) | 90.20(4) | 90.28(5) |
| (Ni,Mo)–O–(Ni,Mo) | 171.94(2) | 171.50(2) | |

Table 4 XPS results of catalysts

| Catalyst | $n$(Ni)/$n$(La+Mg+Al) | $n$(Mg)/$n$(La+Ni+Al) | $n(O_{ad})/n(O_l)$ |
|---|---|---|---|
| $LaMgNi_1$ | 0.048 (0.05)* | 0.05 (0.05) | 0.15 |
| $LaMgNi_2$ | 0.091 (0.11) | 0.07 (0.05) | 0.18 |
| $LaMgNi_3$ | 0.131 (0.176) | 0.095 (0.05) | 0.22 |

*: values between brackets correspond to nominal ones

It has been reported that $LaNiO_3$ perovskite presents three reduction signals at 350, 380 and 500°C, approximately. The first two peaks are assigned to the reduction of $LaNiO_3$ to $La_4Ni_3O_{10}$ and then to $La_2NiO_4$. The third broad peak corresponds to the reduction of $La_2NiO_4$ to $Ni^0$ and $La_2O_3$[26,27]. The similarity in reduction temperatures between NiO and $LaNiO_3$ makes it difficult to correct assign phases. However, the presence of more than two signals in the case of $LaMgNi_y$ perovskites gives evidence of the incorporation of Ni in the perovskite structure. More accurate information could be obtained from $H_2$ consumption data presented in Table 1. It can be observed that perovskites present higher values of $H_2$ consumption than the impregnated sample. This would indicate the presence of $Ni^{3+}$ species together with $Ni^{2+}$. It is also observed a decrease in the consumption with a higher Ni substitution level which would reveal a higher proportion of $Ni^{2+}$ species. Up to now, it could be assumed that part of the Ni is included in the perovskite structure in the three samples, though part of Ni is segregated as NiO especially in $LaMgNi_2$ and $LaMgNi_3$ perovskites. The increase of the first signal intensity could also give evidence of the above explained facts.

In order to elucidate the actual crystalline structure of the perovskite, the samples were studied by neutron powder diffraction (NPD). The refinement of the crystal structure of $La_{0.9}Mg_{0.1}Al_{1-y}Ni_yO_3$ ($y$ = 0.1, 0.2, 0.3) from NPD data, recorded at RT (room temperature) demonstrate that all these samples belong to a rhombohedral polymorph perovskite, which is defined in the space group (no. 167), $Z$ = 6. The unit-cell parameters are listed in Table 3. La and Mg atoms are, at first, distributed at random at 6*a* (0 0 1/4) positions, Al and Ni statistically distributed over the 6*b* (0 0 0) sites and oxygen atoms are at 18*e* ($x$ 0 1/4) positions. After the first stage of the refinement, it is evident that Mg is rejected from the A positions of the $ABO_3$ perovskite, yielding occupancy factors close to 100% for La atoms (Table 2), within the standard deviations. The Al/Ni ratio is also experimentally refined, taking advantage of the high contrast between the scattering lengths for Ni and Al. The refined Ni content is lower than the nominal value, as shown in Table 2. As a consequence of the segregation of MgO and NiO, these oxides are identified in the three NPD patterns and introduced in the refinement as second and third phases, respectively.

Both oxides exhibit a NaCl-type structure, which is defined in the Fm-3m space group, with Ni(Mg) at 1*a* (0 0 0) and O at 1*b* (½ ½ ½). For MgO, $a$ = 4.195(2) Å; for NiO, $a$ = 4.188(2) Å. From the scale factors it is possible to estimate the relative amount of the main perovskite phase and the minor NiO and MgO impurities (Table 2).

Table 2 contains the structural parameters and selected interatomic distances of the main perovskite phases at 25°C. Figure 6 shows the good agreement between the observed and the calculated phases, for the three compositions, $y$ = 0.1, 0.2 and 0.3. A view of the rhombohedral superstructure is shown in Figure 7. After the refinement of the mixed occupancy factors of La/Mg and Al/Ni it is obvious that Mg is not present at the A sublattice, whereas the amount of Ni is progressively increasing at the octahedral B sublattice. Nickel amount incorporated into the $LaAlO_3$ structure is about 66% of the nominal one, which accounts for the presence of NiO as a second phase (together with MgO). It is possible that the total insertion of Ni would require larger pressure of $O_2$, since $LaNiO_3$ contains $Ni^{3+}$ and must be stabilized under high oxygen pressure. As Ni content increases along the series, the unit-cell parameters and volume expand, given a larger ionic size for $Ni^{3+}$ (and $Ni^{2+}$) *vs* $Al^{3+}$ in octahedral coordination. The (Al, Ni)–O bond lengths also increase along the series for the same reason, from 1.9018(7) Å for $y$ = 0.1 to 1.9073(8) Å for $y$ = 0.3 (Table 3). The (Al, Ni)$O_6$ octahedra are slightly distorted with O–Ni–O angles of 90.16(4)º, which slightly increase along the series. The main tilting angle of the (Al, Ni)$O_6$ octahedra, which controls the orbital overlap and hence the electronic transport properties, becomes narrower as temperature increases, from 171.94(2)° for $x$ = 0.1 to 170.81(2)°, as the tolerance factor of the perovskite becomes smaller since the octahedral size increases with Ni incorporation. These structural subtleties are unveiled to the extraordinary precision of the $x$ coordinate for O atoms, determined by neutrons. NPD results corroborate what is supposed by $H_2$-TPR results that a Ni segregation is more evident for a substitution level higher than 0.2. The segregation of Ni as NiO would generate species with different metal support interaction after reduction step, since the nature of Ni species is different. A low metal support interaction is also evident by the shift to low reduction temperatures with the increase of Ni content. These results

also corroborate the absence of a spinel phase as it is supposed by $H_2$-TPR results.

The disposition of this different Ni species on the surface after the reduction procedure can be analysed from the XPS results. XPS data of reduced catalysts are presented in Table 4, and are expressed as atomic ratios of the elements. The partial overlapping between the La $3d_{3/2}$ and Ni $2p_{3/2}$ energy regions makes it difficult to accurately estimate the Ni oxidation state, so Ni 3*p* is analysed. *n*(Ni)/*n*(La+Mg+Al) atomic ratio results are similar to the nominal value for $LaMgNi_1$ perovskite, which indicates that the expulsion of Ni to the surface is reached in a controlled way, repeating the atomic ratio of the crystalline lattice. The same is observed for the *n*(Mg)/*n*(La+Ni+Al) ratio. An increase of *n*(Ni)/*n*(La+Mg+Al) with the increase in Ni content is observed, but these ratios are lower than the nominal ones for $LaMgNi_2$ and $LaMgNi_3$. Thus, the Mg ratio on the surface is slightly higher than the nominal value for these two catalysts. Evidently, the higher NiO/MgO segregation in these two samples modifies the disposition of cations on the surface after the reduction step.

It is also interesting to study the O 1*s* spectrum in order to analyse the presence of oxygen vacancies on the catalysts surface. The O 1*s* spectra of the samples present a main peak at around 530–531 eV. By deconvoluting this peak, two components are distinguished, specifically the low binding energy peak at 529.8–530.1 eV, ascribed to lattice oxygen, $O_l$, ($O_2^{2-}$) and the high binding energy peak 531.3 eV, assigned to surface adsorbed oxygen, $O_{ad}$, ($O^{2-}$ or $O^-$), $OH^-$ groups and oxygen vacancies[29]. The relative abundance of $O_l$ and $O_{ad}$ species are presented in Table 4. As expected, the most abundant component in all samples is the lattice oxygen. It is interesting to note that the $LaAlO_3$ base perovskite evidences the presence of oxygen vacancies, ($n(O_{ad})/n(O_l)$= 0.39) that corroborates what is deduced from $H_2$-TPR results. The increase in Ni content is concomitant to the increment of the oxygen vacancies, which could be explained by the segregation of oxides phases and the incorporation of Ni as $Ni^{2+}$ instead of $Ni^{3+}$ into the perovskite lattice.

The characterization results demonstrate that the better catalytic performance of $LaMgNi_1$ catalyst could be attributed to the minor proportion of segregated phases, and thus a controlled expulsion of Ni phases from the perovskite structure could generate more active species. It is important to note that the inclusion of Mg into the perovskite structure does not allow total inclusion of Ni cations as expected, and evidently there is a limit value of substitution level corresponding to *y*=0.1. However this fact could also demonstrate the importance of the origin of generated Ni particles. The exclusion of Ni from the perovskite structure generates Ni particles with a higher interaction with the support than those generated from segregated NiO phases. It has been demonstrated that a higher interaction of particles with the support could avoid particles sintering which leads to a highly active and stable catalysts as it is demonstrated in this work. This also confirms the importance in catalyst design especially in this reaction where the physicochemical characteristics of the generated particle directly affect its catalytic performance.

## 3 Conclusions

The obtained results show that it is possible to make a proper design of catalysts in the studied reaction. Indeed, high purity $La_{1-x}Mg_xAl_{1-y}Ni_yO_3$ ($x$ = 0.1; $y$ = 0, 0.1, 0.2, 0.3) perovskites with appropriate textural features are obtained. The insertion of Ni in the perovskite structure is confirmed by the increase in the cell parameter of the host perovskite, and corroborated by the $H_2$-TPR and NPD results. However, the segregation of Ni as NiO generates species with different metal support interaction after the reduction step. The methodology used in the synthesis of catalysts is adequate since active catalysts are obtained. The three samples present high activity during 9 h on stream. Total conversion of ethanol is reached in all cases with exceptionally high values of $H_2$ yields. $LaMgNi_1$ catalyst presents the highest $H_2$ yield value, about 85%, during reaction time, with low values of $CH_4$ and CO selectivities of 3.4% and 11%, respectively, and a low carbon formation. The design of catalysts used in steam reforming reaction is essential in order to obtain catalysts with adequate properties in order to favor $H_2$ production and avoid carbon formation. The use of pure perovskites as precursors of Ni leads to catalysts with a high catalytic performance.

## Acknowledgements

The financial support from Universidad Nacional de San Luis, CONICET, ANPCyT is gratefully acknowledge. JAA is grateful to the Spanish Ministry of Economy and Competitivity for granting the project MAT2013-41099-R, and to ILL for making all facilities available for the neutron diffraction experiments.

## References

[1] Chorkendorff I, Niemantsverdriet J W. Concepts of Modern Catalysis and Kinetics. Wiley Editorial, 2003.

[2] Aramouni A K, Touma J G, Tarboush B A, Zeaiter J M. Catalyst design for dry reforming of methane: Analysis review. Renewable Sustainable Energy Rev, 2017, 82(part 3): 2570–2585.

[3] Choi S O, Moon S H. Performance of $La_{1-x}Ce_xFe_{0.7}Ni_{0.3}O_3$ perovskite catalysts for methane steam reforming. Catal Today, 2009, 146(1): 148–153.

[4] Palcheva R, Olsbye U, Palcut M, Rauwel P, Tyuliev G, Velinov N, Fjellväg H H. Rh promoted $La_{0.75}Sr_{0.25}(Fe_{0.8}Co_{0.2})_{1-x}Ga_xO_{3-\delta}$ perovskite catalysts: Characterization and catalytic performance for methane partial oxidation to synthesis gas. Appl Surf Sci, 2015, 357(part A): 45–54.

[5] Ni M, Leung D, Leung M. A review on reforming bio-ethanol for hydrogen production. Int J Hydrogen Energy, 2007, 32(15): 3238–3247.

[6] Pereira E B, Ramírez De La Piscina P, Marti S, Homs N. $H_2$ production by oxidative steam reforming of ethanol over K promoted Co-Rh/$CeO_2$-$ZrO_2$ catalysts. Energy Environ Sci, 2010, 3: 487–493.

[7] Han X, Yu Y, He H, Shan W. Hydrogen production from oxidative steam reforming of ethanol over rhodium catalysts supported on Ce-La solid solution. Int J Hydrogen Energy, 2013, 38(25): 10293–10304.

[8] Costa L O, Vasconcelos S M, Pinto A L, Silva A M, Mattos L V, Noronha F B. Rh/$CeO_2$ catalyst preparation and characterization for hydrogen production from ethanol partial oxidation. J Mater Sci, 2008, 43(2): 440–449.

[9] Kraleva E, Sokolov S, Nasillo G, Bentrup U, Ehrich H. Catalytic performance of CoAlZn and NiAlZn mixed oxides in hydrogen production by bio-ethanol partial oxidation. Int J Hydrogen Energy, 2014, 39(1): 209–220.

[10] Beyhan S, Léger J M, Kadirgan F. Understanding the influence of Ni, Co, Rh and Pd additionto PtSn/C catalyst for the oxidation of ethanol by in situ Fourier transform infrared spectroscopy. Appl Catal B: Environ, 2014, 144: 66–74.

[11] Chen H Q, Yu H, Yang G X, Peng F, Wang H J, Wang J. Auto-thermal ethanol micro-reformer with a structural Ir/$La_2O_3$/$ZrO_2$ catalyst for hydrogen production. Chem Eng J, 2011, 167(1): 322–327.

[12] Silva A M, Costa L O, Barandas A P, Borges L E, Mattos L V, Noronha F B. Effect of the metal nature on the reaction mechanism of the partial oxidation of ethanol over $CeO_2$-supported Pt and Rh catalysts. Catal Today, 2008, 133–135: 755–761.

[13] Frusteri F, Freni S. Bio-ethanol, a suitable fuel to produce hydrogen for a molten carbonate fuel cell. J Power Sources, 2007, 173(1): 200–209.

[14] Bion N, Epron F, Duprez D. Bioethanol reforming for $H_2$ production. A comparison with hydrocarbon reforming. Catalysis, 2010, 22: 1–55.

[15] Haryanto A, Fernando S, Murali N, Adhikari S. Current status of hydrogen production techniques by steam reforming of ethanol: A review. Energy Fuels, 2005, 19(5): 2098–2106.

[16] Bengaard H S, Norskov J K, Sehested J, Clausen B S, Nielsen L P, Molenbroek A M, Rostrup-Nielsen J R. Steam reforming and graphite formation on Ni catalysts. J Catal, 2002, 209(2): 365–384.

[17] Borowiecki T. Nickel catalysts for steam reforming of hydrocarbons; size of crystallites and resistance to coking. Appl Catal, 1982, 4: 223–231.

[18] Agüero F, Morales M R, Larregola S, Izurieta E, Lopez E, Cadus L E. $La_{1-x}Ca_xAl_{1-y}Ni_yO_3$ perovskites used as precursors of nickel based catalysts for ethanol steam reforming. Int J Hydrogen Energy, 2015, 40: 15510.

[19] Courty P, Ajot H, Marcilly C, Delmon B. Oxydes mixtes ou en solution solide sous forme très divisée obtenus par décomposition thermique de précurseurs amorphes. Powder Technol, 1973, 7(1): 21–38.

[20] Rietveld H M. A profile refinement method for nuclear and magnetic structures. Appl Crystallogr, 1969, 2: 65–71.

[21] Rodríguez-Carvajal J. Recent advances in magnetic-structure determination by neutron power diffraction. Phys B, 1993, 192(1/2): 55–69.

[22] Wu Y J, Díaz Alvarado F, Santos J C, Gracia F, Cunha A F, Rodrigues A E. Sorption-enhanced steam reforming of ethanol: Thermodynamic comparison of $CO_2$ sorbents. Chem Eng Technol, 2012, 35(5): 847–858.

[23] Cunha A F, Wu Y J, Díaz Alvarado F A, Santos J C, Vaidya P D, Rodrigues A E. Steam reforming of ethanol on a Ni/$Al_2O_3$ catalyst coupled with a hydrotalcite-like sorbent in a multilayer pattern for $CO_2$ uptake. Can J Chem Eng, 2012, 90(6): 1514–1526.

[24] Sánchez-Sánchez M C, Navarro R M, Fierro J L G. Ethanol steam reforming over Ni/$M_xO_y$-$Al_2O_3$ (*M*¼Ce, La, Zr and Mg) catalysts: Influence of support on the Hydrogen production. Int J Hydrogen Energy, 2007, 32: 1462.

[25] Hardini D, Yoon C, Hon J, Yoon S, Nam S, Lim T. Influence of preparation methods and OSC on activity and stability. Catal Lett, 2012, 142(2): 205–212.

[26] Ribeiro N, Neto R, Moya S, Souza M, Schmal M. Synthesis of $NiAl_2O_4$ with high surface area as precursor of Ni nanoparticles for hydrogen production. Int J Hydrogen Energy, 2010, 35(21): 11725–11732.

[27] Gallego G S, Mondragón F, Barrault J, Tatibouët J-M, Batiot-Dupeyrat C. $CO_2$ reforming of $CH_4$ over La-Ni based perovskite precursors. Appl Catal A: Gen, 2006, 311(1): 164–171.

[28] Sierra Gallego G, Mondragon F, Tatibouët J M, Barrault J Batiot-Dupeyrat C. Carbon dioxide reforming of methane over $La_2NiO_4$ as catalyst precursor and characterization of carbon deposition. Catal Today, 2008, 133–135: 200–209.

[29] Jiratova K, Mikulova J, Klempa J, Grygar T, Bastl Z, Kovanda F. Modification of Co-Mn-Al mixed oxide with potassium and its effect on deep oxidation of VOC. Appl Catal A: Gen, 2009, 361: 106–116.